Anal. Chem. **2007,** *79,* 6682−6689

High-Throughput DNA Droplet Assays Using Picoliter Reactor Volumes

Monpichar Srisa-Art,[†] Andrew J. deMello,*[,†] and Joshua B. Edel*[,†,‡]

Department of Chemistry and Institute of Biomedical Engineering, Imperial College London, South Kensington, London, SW7 2AZ, United Kingdom

The online characterization and detection of individual droplets at high speeds, low analyte concentrations, and perfect detection efficiencies is a significant challenge underpinning the application of microfluidic droplet reactors to high-throughput chemistry and biology. Herein, we describe the integration of confocal fluorescence spectroscopy as a high-efficiency detection method for droplet-based microfluidics. Issues such as surface contamination, rapid mixing, and rapid detection, as well as low detections limits have been addressed with the approach described when compared to conventional laminar flow-based fluidics. Using such a system, droplet size, droplet shape, droplet formation frequencies, and droplet compositions can be measured accurately and precisely at kilohertz frequencies. Taking advantage of this approach, we demonstrate a high-throughput biological assay based on fluorescence resonance energy transfer (FRET). By attaching a FRET donor (Alexa Fluor 488) to streptavidin and labeling a FRET acceptor (Alexa Fluor 647) on one DNA strand and biotin on the complementary strand, donor and acceptor molecules are brought in proximity due to streptavidin−biotin binding, resulting in FRET. Fluorescence bursts of the donor and acceptor from each droplet can be monitored simultaneously using separate avalanche photodiode detectors operating in single photon counting mode. Binding assays were investigated and compared between fixed streptavidin and DNA concentrations. Binding curves fit perfectly to Hill−Waud models, and the binding ratio between streptavidin and biotin was evaluated and found to be in agreement with the biotin binding sites on streptavidin. FRET efficiency for this FRET pair was also investigated from the binding results. Efficiency results show that this detection system can precisely measure FRET even at low FRET efficiencies.

In recent years, microfluidic systems have been successfully used to generate multiphase flows in a variety of formats. Of particular note are those that exploit flow instabilities between immiscible fluids to generate suspended droplets.[1] In simple terms, droplets can be made to spontaneously form when laminar streams of aqueous reagents are injected into an immiscible carrier fluid. The formed droplets define picoliter volumes, and because each droplet is isolated from both channel surfaces and other droplets, each acts as an individual reaction vessel.[2] Importantly, variation of the cross-sectional dimensions of the microfluidic system and the relative flow rates of the input streams allows for exquisite control over droplet size, volume fraction in the continuous phase, frequency of droplet production, and relative concentrations of reagents contained within each droplet. Several recent studies have exploited the formation of droplets in microfluidic systems to perform a variety of analytical processes.[2] For example, droplet-based microfluidic systems have been used to perform enzyme assays,[3] small-molecule synthesis,[4−6] protein crystallization,[7−9] nanoparticle synthesis,[10−12] enzyme kinetic studies,[13] synthesis of functional reaction networks,[6] and cell-based assays.[14] Droplet-based microfluidic systems provide a controlled environment in which to perform rapid mixing, isolation of picoliter-size fluid volumes, and rapid variation of reaction conditions. An elegant example of this facility has been demonstrated by Ismagilov and colleagues, in which they used droplets to measure reaction kinetics on the millisecond time scale.[1] The rapid binding rate of Ca^{2+} to fluoro-4, a calcium-sensitive dye, which is strongly fluorescent when combined with Ca^{2+}, was measured using a

* To whom correspondence should be addressed. E-mail: a.demello@imperial.ac.uk, joshua.edel@imperial.ac.uk.

† Department of Chemistry.

‡ Institute of Biomedical Engineering.

(1) Song, H.; Tice, J. D.; Ismagilov, R. F. *Angew. Chem., Int. Ed.* **2003**, *42*, 768−772.

(2) Song, H.; Chen, D. L.; Ismagilov, R. F. *Angew. Chem., Int. Ed.* **2006**, *45*, 7336−7356.

(3) Zheng, B.; Ismagilov, R. F. *Angew. Chem., Int. Ed.* **2005**, *44*, 2520−2523.

(4) Hatakeyama, T.; Chen, D. L. L.; Ismagilov, R. F. *J. Am. Chem. Soc.* **2006**, *128*, 2518−2519.

(5) Cygan, Z. T.; Cabral, J. T.; Beers, K. L.; Amis, E. J. *Langmuir* **2005**, *21*, 3629−3634.

(6) Bringer, M. R.; Gerdts, C. J.; Song, H.; Tice, J. D.; Ismagilov, R. F. *Philos. Trans. R. Soc. London Ser. A: Math. Phys. Eng. Sci.* **2004**, *362*, 1087−1104.

(7) Zheng, B.; Roach, L. S.; Ismagilov, R. F. *J. Am. Chem. Soc.* **2003**, *125*, 11170−11171.

(8) Zheng, B.; Tice, J. D.; Ismagilov, R. F. *Adv. Mater.* **2004**, *16*, 1365−1368.

(9) Yadav, M. K.; Gerdts, C. J.; Sanishvili, R.; Smith, W. W.; Roach, L. S.; Ismagilov, R. F.; Kuhn, P.; Stevens, R. C. *J. Appl. Crystallogr.* **2005**, *38*, 900−905.

(10) Shestopalov, I.; Tice, J. D.; Ismagilov, R. F. *Lab Chip* **2004**, *4*, 316−321.

(11) Chan, E. M.; Alivisatos, A. P.; Mathies, R. A. *J. Am. Chem. Soc.* **2005**, *127*, 13854−13861.

(12) Hung, L. H.; Choi, K. M.; Tseng, W. Y.; Tan, Y. C.; Shea, K. J.; Lee, A. P. *Lab Chip* **2006**, *6*, 174−178.

(13) Song, H.; Ismagilov, R. F. *J. Am. Chem. Soc.* **2003**, *125*, 14613−14619.

(14) Huebner, A.; Srisa-Art, M.; Holt, D.; Abell, C.; Hollfelder, F.; deMello, A. J.; Edel, J. B. *Chem. Commun.* **2007**, 1218−1220.

10.1021/ac070987o CCC: $37.00
Published on Web 08/04/2007

winding poly(dimethylsiloxane) (PDMS) channel to accelerate fluidic mixing. Results showed that strong fluorescence associated with the mixing of Ca^{2+} and fluoro-4 inside the droplets was due to the formation of fluoro-4−Ca^{2+}. This reaction was observed over a distance of 500 μm. In addition, at higher flow rates, mixing times as fast as 2 ms were achieved. In addition, Huebner et al. recently reported the encapsulation of single cells within microdroplets to allow for high-throughput screening of *Escherichia coli* cells. In this study, cells expressing a fluorescent protein were controllably encapsulated in droplets, with cell load, droplet size, and droplet generation frequencies monitored in real time.[14]

In all situations, the ability to controllably form droplets with variable reagent composition at high-speed lies at the heart of the performance improvements when compared to conventional microfluidic devices operating under laminar flow conditions. It is interesting to realize that segmented-flow systems can generate droplets at rates in excess of 1 kHz. In theory, this means that millions of individual reactions or assays can be processed in very short times. Nevertheless, few—if any—studies have successfully exploited this unique feature, with analytical throughput normally defined by the speed at which the detection system can function. Although a range of detection methods have been used to characterize droplets, almost all reported studies incorporate fluorescence detection using a microscope equipped with a CCD camera. Unfortunately, at high droplet generation rates, conventional CCD cameras are not fast enough to sensitively interrogate each droplet. Accordingly, more costly high-speed cameras (typically with frame speeds in excess of 1000 frames/s) are typically used; however, these cameras lack sensitivity when compared to photomultiplier tubes and avalanche photodiode detectors (APDs), which both have high sensitivity[15] and fast response times.

Accordingly, an efficient detection system for extracting and utilizing the vast amounts of information produced from microdroplet reactors is certain to be key in defining the ultimate utility of segmented-flow systems in high-throughput chemistry and biology.[16] To this end, we report herein, a high-sensitivity confocal fluorescence detection system integrated with droplet-based microfluidic devices to conduct high-throughput biological assays. Through the integration of high-sensitivity confocal fluorescence spectroscopy, we demonstrate that online characterization of picoliter-sized droplets in continuous-flow and high-speed droplet generation rates can be performed and that analyte inside such droplets can be accurately and precisely quantified in a high-throughput format. Moreover, we use this approach to perform a high-speed and low-volume biological assay based on fluorescence resonance energy transfer (FRET) spectroscopy. The application of such a format is especially advantageous since analyte confinement and isolation within droplets removes any possibility of surface adsorption and other forms of contamination that afflict conventional, single-phase laminar flow systems. In addition, since mixing is rapid and reagent transport occurs with no dispersion, microdroplet reactors are superior environments in which to study reaction kinetics when compared to diffusion-limited, continuous-flow formats.

(15) Stavis, S. M.; Edel, J. B.; Li, Y. G.; Samiee, K. T.; Luo, D.; Craighead, H. G. *Nanotechnology* **2005**, *16*, S314−S323.
(16) deMello, A. J. *Nature* **2006**, *442*, 394−402.

EXPERIMENTAL SECTION

Device Fabrication and Operation. Microfluidic devices were fabricated by PDMS molding from SU-8 masters.[17] Access holes were punched into the PDMS channel ends with a syringe needle. To yield rigid microfluidic test devices, 1-mm-thick microscope slides were used as a chip-to-world interface. Holes coinciding with access holes in the PDMS microfluidic layer were drilled with a 1-mm-diameter diamond drill bit. Standard fused-silica capillaries (150-μm i.d., 375-μm o.d., Composite Metal Services, Hallow, UK) were then inserted and fixed with chemically resistant epoxy to serve as fluidic reservoirs (Araldite 2014, RS Components, Corby, UK). For optical imaging, the PDMS microdevice was attached to a 160-μm microscope coverslip. The microchip layout comprises either three or four inlets, a 50-μm-wide and 50-μm-deep mixing channel, and a common outlet. This design broadly follows the layout originally described by Song et al.[1] A section of the PDMS microfluidic device is shown in Figure 1a. It should also be noted that an initial winding section (not shown) of the primary microchannel was integrated to induce chaotic advection inside droplets and thus allow extremely rapid and efficient mixing within each droplet.[6,18]

Detection System. The completed microfluidic device was placed onto a translation stage and appropriately aligned with a custom-built confocal spectrometer[19] (Figure 1b). Briefly, the spectrometer consisted of a 488-nm CW air-cooled argon ion laser excitation source. A dichroic mirror (505DRLP02; Omega Optical, Brattleboro, VT) is used to reflect the 488-nm radiation and so define a vertical axis, normal to the surface of the optical table. A 100× microscope objective brings the light to a tight focus within the microfluidic channel. Subsequently, fluorescence emission is collected with the same high-NA objective and transmitted through the same dichroic mirror. An emission filter (515EFLP; Omega Optical) removes any residual excitation light, and a plano-convex lens (+50.2F; Newport Ltd.) focuses the fluorescence onto a precision pinhole (200 μm; Melles Griot, Huntingdon, Cambridgeshire, UK). Another long-pass dichroic mirror (630 LP) is then used to split the signal onto two avalanche photodiodes (AQR-141, EG&G, Perkin-Elmer). Dual detection was implemented for FRET-based experiments where the Alexa 488 and Alexa 647 fluorophores are recorded in distinct detection channels. Both detectors are coupled to a multifunction DAQ device for data logging (National Instruments, USB-6251) and have sub-microsecond time resolution per channel.

It should be noted that the instrumentation described can easily be adapted for use with a slit scanning geometry to improve overall concentration detection limits further. Nevertheless, in the current embodiment, the detection system has single molecule/fluorophore resolution and consists of a diffraction-limited Gaussian probe volume. Accordingly, if desired, local intradroplet variations can be monitored with high spatial resolution.

Sample Preparation. Alexa Fluor 488 streptavidin conjugate was obtained from Invitrogen (Paisley, UK). Oligonucleotides were

(17) McDonald, J. C.; Whitesides, G. M. *Acc. Chem. Res.* **2002**, *35*, 491−499.
(18) Song, H.; Bringer, M. R.; Tice, J. D.; Gerdts, C. J.; Ismagilov, R. F. *Appl. Phys. Lett.* **2003**, *83*, 4664−4666.
(19) Edel, J. B.; Hill, E. K.; de Mello, A. J. *Analyst* **2001**, *126*, 1953−1957.

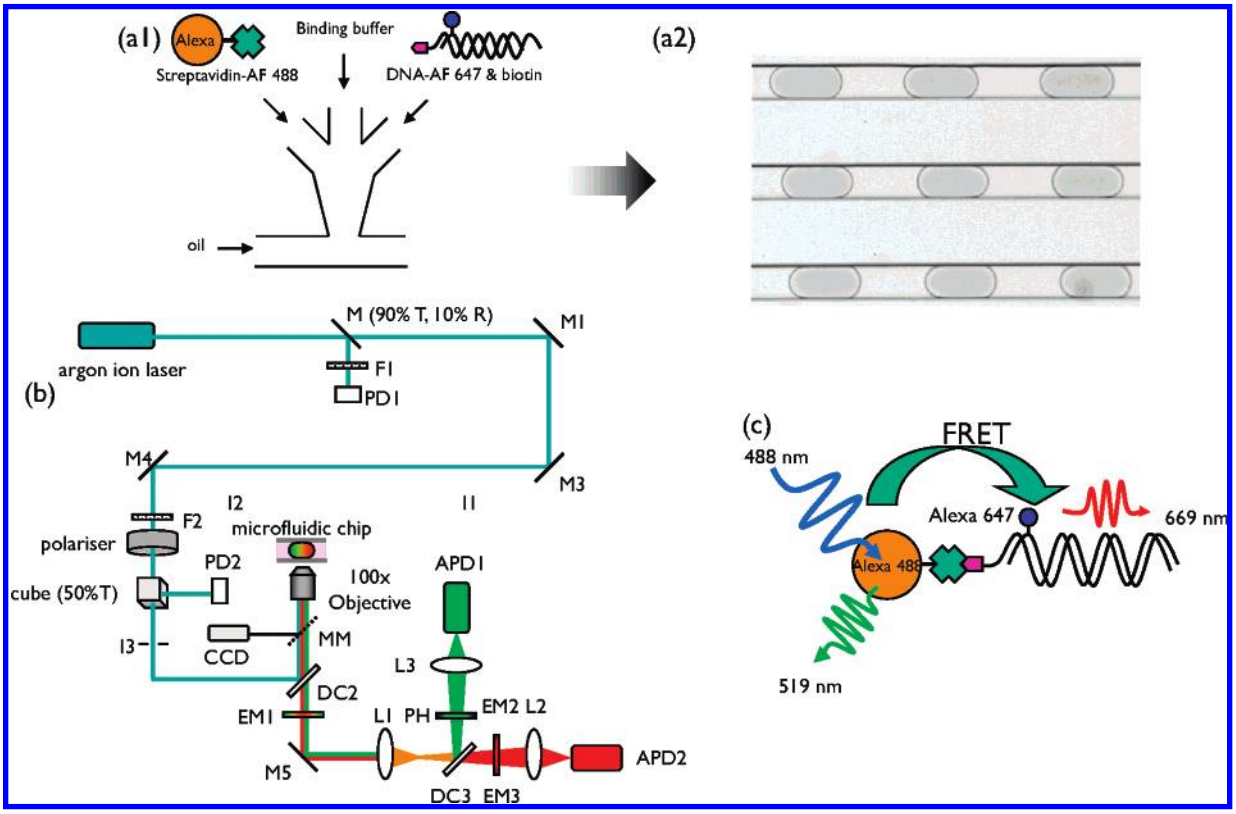

Figure 1. (a1) Schematic of the microfluidic device. The 50-μm square cross-section microchannel network consists of 4 inlets and 1 outlet. The 3 aqueous inlets used in the assay consist of a binding buffer, strepatavidin, and biotinylated DNA. (a2) Example image of droplets generated using the microfluidic system. (b) Schematic of the optical detection system used. A complete description of the setup is supplied in Supporting Information. (c) Schematic of the Alexa 488−Alexa 647-labeled DNA FRET system. The donor, Alexa 488, is conjugated with streptavidin. The acceptor, Alexa 647, is labeled on one DNA strand and the complementary strand is labeled with biotin. The acceptor is linked to the donor via the streptavidin−biotin linkage.

purchased from Operon (Cologne, Germany). The biotinylated strand consisted of the following sequence: biotin-5′-GCGCTAAAATTATTTATTGATCGATTTTTTTTCGGGCGCGGCGGGC-3′. A complementary strand internally modified with Alexa Fluor 647 possesses the sequence 3′-CGCG[Alexa 647]TTTTAATA AATAACTAGCTAAAAAAAAGCCCGCGCCGCCCG-5′. DNA hybridization was conducted at pH 8.0 using a binding buffer consisting of 100 mM Tris-HCl, 10 mM NaCl, and 3 mM $MgCl_2$. A mixture of single-stranded DNA (biotin-labeled DNA and Alexa 647-labeled DNA) was prepared by pipetting 50 μL of 200 nM of each DNA solution into 200-μL Eppendorf tubes, resulting in each DNA strand having a concentration of 100 nM. The DNA mixture was hybridized using a Genius Thermal Cycler (Techne, Cambridge, UK). Hybridization was performed by rapidly increasing the temperature to 92 °C and holding at this temperature for 2 min. The temperature was then slowly decreased to 4 °C at a rate of 1.6 °C min^{-1}.

To perform the high-throughput DNA binding assay, Alexa Fluor 488 conjugated with streptavidin and Alexa Fluor 647 coupled to DNA was used as a FRET donor and acceptor pair, respectively. One of the two DNA sequences was labeled with Alexa Fluor 647 and the other with biotin. Consequently, hybridized DNA consisted of Alexa Fluor 647 on one strand and biotin on the complementary strand. The acceptor (Alexa Fluor 647) was linked to the donor (Alexa Fluor 488) via a biotin−streptavidin linkage. Sections a and c in Figure 1 schematically show a microfluidic device setup for FRET experiments and how the FRET process occurs, respectively. The Förster distance R_0 (the distance at which FRET efficiency is 50%) of this FRET pair was estimated to be 39.0 Å on the basis of Förster formalism.[20] The donor−acceptor distance (R_{DA}) was found to be ~41.6 Å, calculated using a distance of 13.6 Å for the four-base pair separation between the donor and acceptor and the radii of streptavidin (25.0 Å) and biotin (3.0 Å).[21]

Fluidics. Precision syringe pumps (PHD 2000, Harvard Apparatus) were used to deliver reagent solutions at flow rates ranging from 0.1 to 5 μL min^{-1} using 1-mL gastight syringes (SGE Europe Ltd.). The continuous oil phase used for all experiments consisted of a 10:1 (v/v) mixture of perfluorodecalin and 1*H*,1*H*,2*H*,2*H*-perfluorooctanol. All liquids were filtered using 0.2-μm syringe filters (Pall Corp.) before use.

RESULTS AND DISCUSSION

Preliminary characterization experiments were conducted using fluorescein 5-isothiocyanate (FITC) in a pH 9.0 buffer, with droplets being generated within two aqueous-inlet microfluidic devices. The FITC solution and pH 9.0 buffer were introduced separately via the two aqueous inlets. Accordingly, online dilution can be performed by changing the relative flow rates of FITC and buffer streams, but keeping the total aqueous flow rate constant to maintain the water fraction. FITC fluorescence was detected

(20) Clapp, A. R.; Medintz, I. L.; Mauro, J. M.; Fisher, B. R.; Bawendi, M. G.; Mattoussi, H. *J. Am. Chem. Soc.* **2004**, *126*, 301−310.
(21) Swift, J. L.; Heuff, R.; Cramb, D. T. *Biophys. J.* **2006**, *90*, 1396−1410.

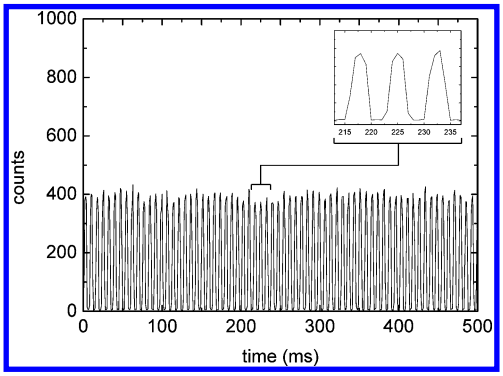

Figure 2. Optical readout of 500-ms window for droplets containing a 53.3 mM solution of FITC in a pH 9.0 buffer. This experiment was carried out using total flow rate of 7.5 μL min^{-1} (50 mm s^{-1}) and Wf = 0.5. Each fluorescence peak corresponds to an individual droplet, and data were recorded using 1-ms bin time. The inset defines an expanded 20-ms portion of the main trace.

by the green APD detector at 1-ms resolution for a 65-s acquisition time.

Figure 2 shows representative data over a period of 500 ms for 53.3 μM FITC at a volumetric flow rate of 3.75 μL min^{-1} (for both the aqueous and oil phases). The total flow rate was 7.5 μL min^{-1}, corresponding to a linear flow velocity of 50.0 mm s^{-1} and a water fraction of 0.5. For the current experiments, the water fraction (W_f) is simply defined as $W_f = F_w/(F_w + F_o)$, where F_w and F_o are the total aqueous- and oil-phase flow rates, respectively. The uniformity of the droplet signature is highlighted by an expanded segment shown in the inset of Figure 2. Average signal intensities were typically on the order of ~400 counts. The relative standard deviation was determined to be ~4.1%. In general, the fluorescent signal recorded was highly uniform, confirming that droplet generation, as well as delivery of the aqueous and oil phases within the microfluidic structure, was highly reproducible in nature. It should also be noted that since variation of the incident laser intensity plays a significant role in accurate determination of burst heights, a photodiode was used to correct for any instabilities associated with the laser output. The diffraction-limited focus of the laser beam was aligned directly to the central portion of the channel width. Moreover, expanding the laser beam further to probe the entirety of the droplet can in principle decrease the spread in the burst heights; however, this was not performed in the current experiments to ensure a sufficiently high signal-to-noise ratio (SNR) at low analyte concentrations. In practice, decreasing the width of the channel should allow for a larger percentage of the droplet to be probed while maintaining sufficiently high contrast in terms of SNR. These experiments will be investigated in a further study.

An average background signal intensity of 10.2 counts per bin for flow rates ranging from 0.1 to 8.0 μL min^{-1} remains approximately constant throughout each acquisition. The background threshold was therefore set to 10 counts per bin for all experiments as predicted by a Poissonian analysis. A photon counting histogram (PCH) was used as the starting point for determining an appropriate threshold for a given data set. Since the background shot noise exhibits Poissonian statistics,[22] the early part of the PCH (dominated by low, background counts) is modeled to a Poisson distribution, which then sets a statistical limit for the droplet threshold. Photon counting events above this threshold were identified as droplets. In an analogy with Gaussian systems, the selected peak discrimination threshold can be defined as three standard deviations from the mean background count rate. Adoption of this threshold yields a confidence limit that is greater than 99% in discriminating between signal and noise.

An example of a time trace for three different dilutions over a 200-ms window is shown in Figure 3a. The volumetric flow rates in the aqueous channel were varied to change to the total FITC concentration after mixing. Importantly, the flow rates can be changed on-the-fly resulting not only in high-throughput droplet generation but also in local conditional changes within a droplet. The total aqueous flow rate in this example was kept constant at 3.0 μL min^{-1}, and the FITC flow rate was gradually increased from 0.3 to 0.9 and 1.5 μL min^{-1} resulting in peak intensities of 184, 515, and 882 counts, respectively. The uniformity of droplet size and the reproducibility in the rate of formation can be assessed by performing a Fourier transform (FT) of the time-domain fluorescent readout. An example of such an analysis is shown in Figure 3b for an acquisition period of 65 s and FITC concentrations of 100, 300, and 500 nM. The greater the variation in droplet size and droplet generation rates, the broader the full width at half-maximum (fwhm) of the FT. The droplet frequency was 70 Hz with a fwhm less than 1 Hz, indicating a polydispersity less than 5%. As expected, nonuniform droplet generation will severely broaden the fwhm. For our system, this is only observed if unstable flows caused by channel blockage or leakage at the syringe/capillary interface occur.

To further observe the stability of droplet formation and the efficiency of the detection system, compositions of aqueous solutions inside the droplets were changed by continuously varying the volumetric flow rates of the aqueous solutions, to ramp the FITC concentration from 100 to 60 000 nM. The total aqueous flow rate was kept constant at 3.0 μL min^{-1} and the oil flow was maintained at 4.5 μL min^{-1}, resulting in a water fraction of 0.4. Fluorescence emission of FITC from each droplet was recorded using 1-ms bin times over a period of 65 s. A calibration plot of FITC concentration as a function of burst height is shown in Figure 4a. The relationship between burst height and FITC concentration is seen to be linear with a high correlation coefficient of $R^2 = 0.9981$. In addition, droplet widths and frequencies were determined throughout the FITC concentration range. Inspection of Figure 4b and c shows that droplets were ~10 ms in length and were produced at a rate of 68 Hz with a relative standard deviation of less than 3%. These data indicate high uniformity and stability of droplet size and high reproducibility in formation rate.

Subsequently, we applied the system to perform a biotin/streptavidin assay based on FRET. The assay was performed using three aqueous-inlet microfluidic devices having 50-μm width, 50-μm depth, and ~44-cm length. A schematic of this device is shown in Figure 1a. The flow rates of the oil phase and aqueous solutions were set to 1.5 μL min^{-1}, resulting in a total flow rate of 3.0 μL min^{-1} (20 mm s^{-1}) and a water fraction of 0.5. Streptavidin

(22) Edel, J. B.; deMello, A. J. *Appl. Phys. Lett.* **2007**, *90*, 053904.

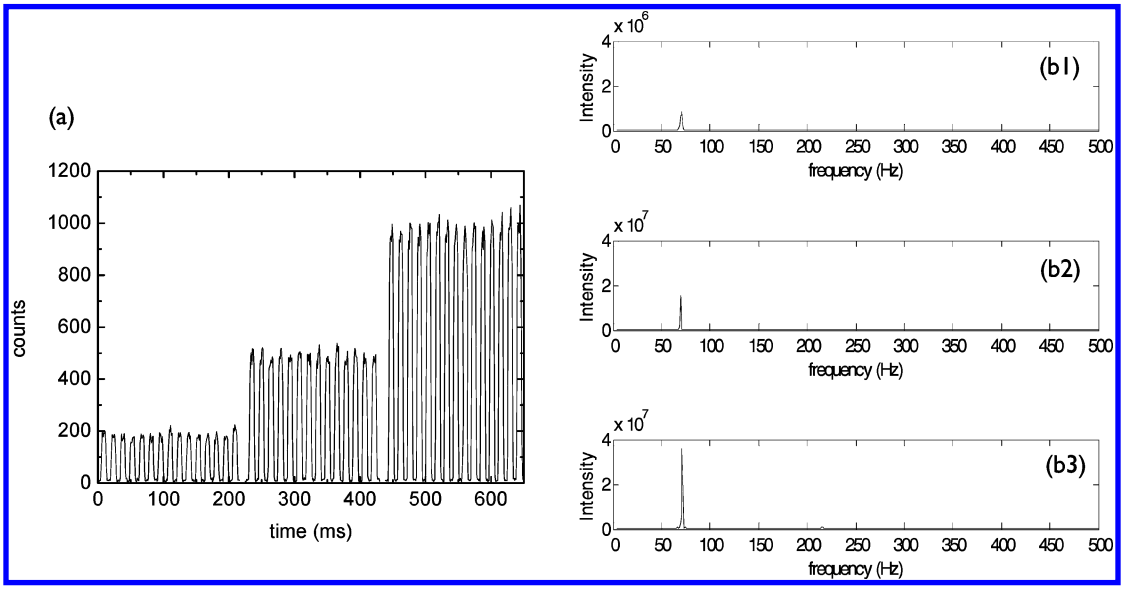

Figure 3. (a) Optical readout for 3 different FITC concentrations (100, 300, and 500 nM) over a 650-ms window. Droplets were produced using oil and aqueous flow rates of 4.5 and 3.0 μL min^{-1}, respectively, resulting in the total flow rate of 7.5 μL min^{-1} (50 mm s^{-1}) and water fraction of 0.4. (b) FTs of the time-domain fluorescent readouts of the same data presented in (a): (b1) 100, (b2) 300, and (b3) 500 nM.

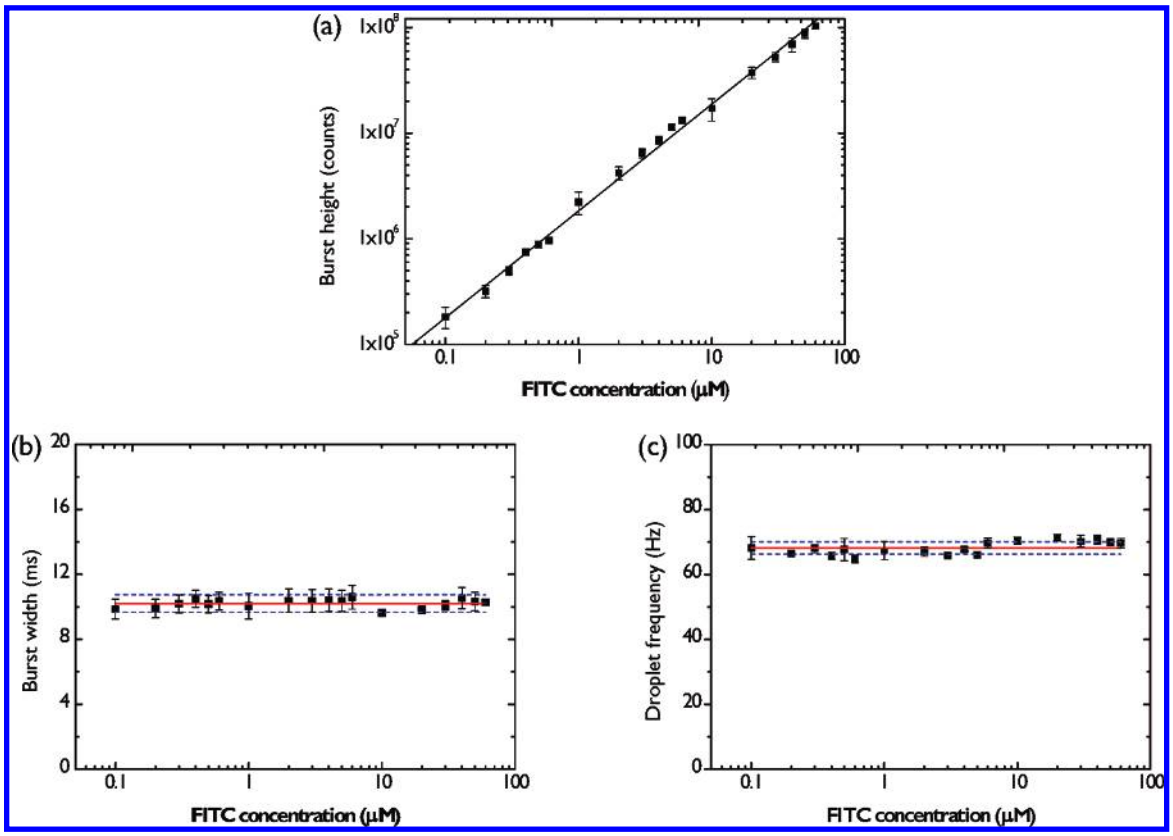

Figure 4. Variation of fluorescence burst height (a), droplet frequency (b), and burst width (c) as a function of FITC concentration. Solid red lines and dashed blue dash lines in (b) and (c) represent the values of mean and one standard deviation from the mean, respectively. Fluorescence bursts were collected over a period of 65 s with a temporal resolution of 1 ms. Droplet formation conditions are as shown in Figure 3.

conjugated with Alexa 488 and Alexa 647-labeled hybridized DNA solutions in binding buffer were pumped separately through the aqueous inlets. Binding buffer was delivered into the middle aqueous inlet to prevent the reagents from coming into contact prior to droplet formation. Thus, mixing and binding of streptavidin and DNA only occurs inside the formed droplet. Since Alexa 488 emits green fluorescence with a peak maximum at 519 nm, upon binding of streptavidin to biotin, some energy is transferred to Alexa 647. Red fluorescence, detected by the acceptor APD detector, at wavelengths between 650 and 710 nm, was obtained from Alexa 647 emission only as a result of FRET. Thus, two fluorescence signals, from Alexa Fluor 488 and Alexa Fluor 647,

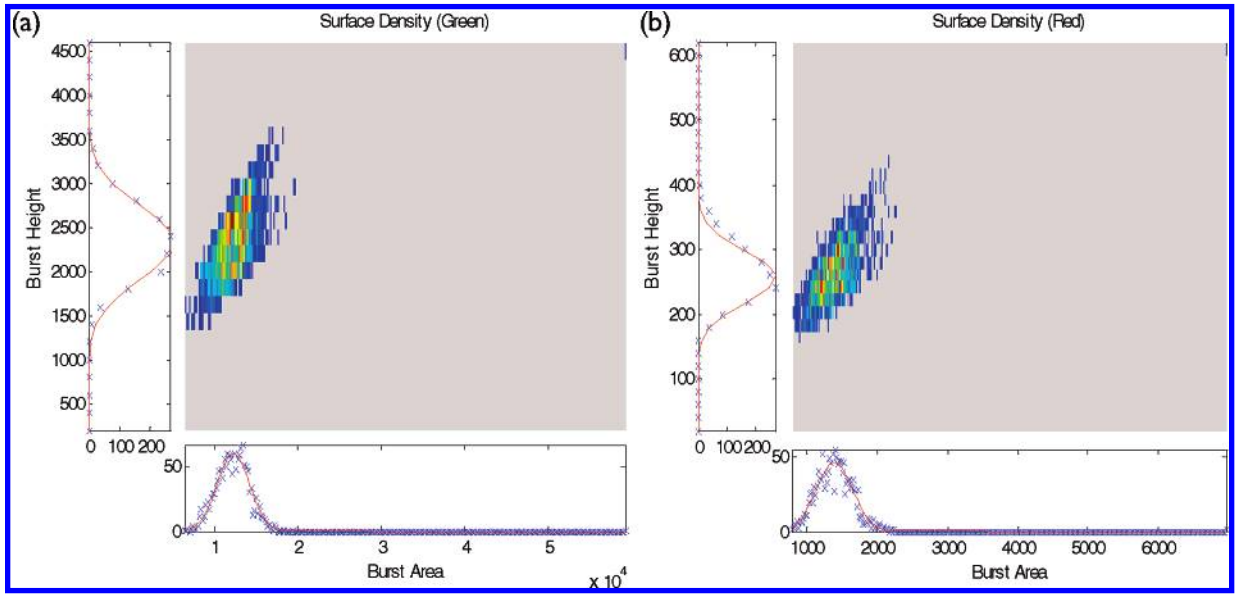

Figure 5. Graphical representation of FRET distributions. Surface density plots of burst height and area for green (a) and red (b) channels. Fluorescence bursts were recorded using 50-ms resolution over a 60-s acquisition time.

were detected simultaneously using separate APD detectors and recorded for 60 s using 50-μs bin times.

In order for efficient FRET, the donor emission spectrum must overlap with the acceptor absorption spectrum. The greater the spectral overlap, the higher the FRET efficiency. However, cross talk (leakage of donor emission into the acceptor detector) must be minimized. Hence, the FRET efficiency and leakage have to be carefully balanced. Furthermore, direct excitation of the acceptor must be eliminated. Therefore, Alexa Fluor 488 and Alexa Fluor 647 were selected as the FRET pair in this system in order to minimize cross talk and avoid direct excitation of the acceptor. Due to the high sensitivity of the APD detectors, fluorescence from FRET can be detected accurately and precisely even at low FRET efficiency. It was found that cross talk of this FRET pair was only ~1.2%. However, for precise determination of fluorescence intensities, photon counts from the acceptor detector were corrected using the following relationship:

$$I'_A = I_A - \left(I_{DNA} \times \frac{C'_{DNA}}{C_{DNA}}\right) - \left(I_{St} \times \frac{C'_{St}}{C_{St}}\right) \quad (1)$$

Here I_A and I'_A are photon counts from the acceptor (red) detector before and after correction, I_{DNA} and I_{St} are photon counts from the acceptor detector when using only DNA and streptavidin (no FRET), respectively. C is the initial concentration, and C' is the concentration for each condition in the experiment.

An initial assay was conducted by fixing the donor-labeled streptavidin concentration and varying the acceptor-labeled DNA concentration. This was achieved by keeping the flow rate of 110 nM streptavidin constant, while varying the flow rate of 100 nM DNA. The flow rate of the binding buffer was changed to maintain a total aqueous flow rate of 1.50 μL min^{-1}. To study the effects of fixed streptavidin concentrations on binding curves, the fixed flow rate of streptavidin was changed from 0.20 to 0.30 μL min^{-1} to obtain 14.7 and 22.0 nM streptavidin concentrations. For each streptavidin flow rate, the same set of DNA flow rates (varied from 0.10 to 1.10 μL min^{-1}) was used to enable comparison of binding results. Consequently, binding ratios, defined as the ratio of DNA concentration to streptavidin concentration, were slightly different for each streptavidin concentration. Taking advantage of the microfluidic approach used, concentrations of each solution were precisely and continuously varied by changing the flow rates of the syringe pumps. In addition, the same set of binding ratios (varied from 0.30 to 3.33) was used for each streptavidin flow rate (0.20 and 0.30 μL min^{-1}). Importantly, the green and red signals are co-incident, indicating that within droplets efficient transferral of energy between donor and acceptor occurs.

Extracted burst heights and areas of both the green and red fluorescence signals were plotted as surface densities (Figure 5a and b) to allow inspection of data distributions for ~2600 droplets. Both are perfectly modeled by Gaussian distributions with well-defined fwhm and confirm high reproducibility and small dispersion of burst heights and widths for both green and red channels. Droplet widths obtained from the donor (green) and acceptor (red) detectors were in excellent agreement. The average droplet size was found to be 30 ms with a relative standard deviation of ~10%.

Binding curves illustrating the binding ratio as a function of fluorescence burst height from the acceptor detector (red detector) are presented in Figure 6a. For each fixed streptavidin concentration at 14.7 and 22.0 nM, "red" fluorescence bursts increase with the binding ratio. This is a result of greater energy transfer with a higher number of acceptors linked to the donor. However, further increases in binding ratio (above 2.0) did not result in higher fluorescence bursts due to the limitation of biotin-binding sites on the streptavidin-conjugated Alexa 488. Comparison of data measured at different streptavidin concentrations demonstrates that the higher the streptavidin concentration, the higher the energy transfer (due to the increased number of donors to transfer energy). It was observed that all binding curves plateau at binding ratios of ~2.0, indicating that only two biotin-binding sites on streptavidin were successfully filled.

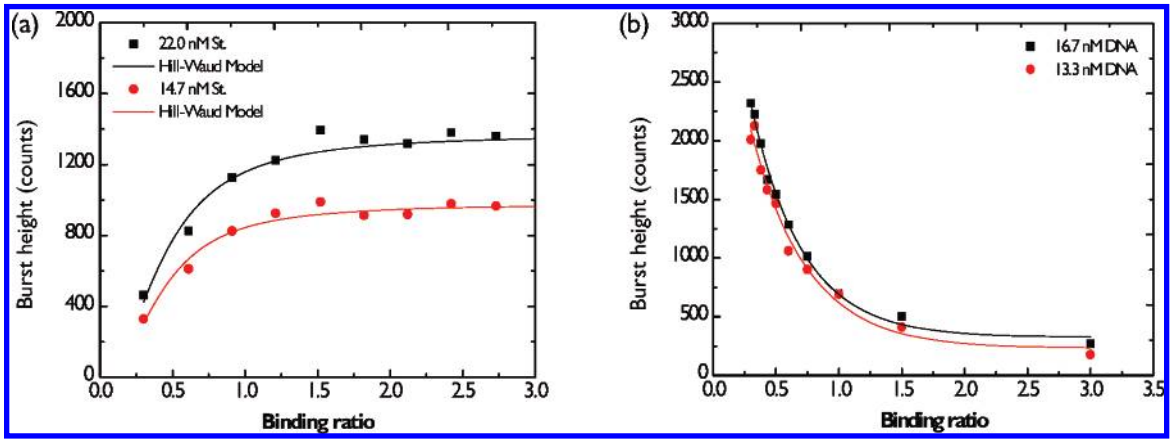

Figure 6. Binding curves illustrating the binding ratio as a function of fluorescence burst height from the acceptor detector. (a) Plot of red fluorescence burst height from FRET against binding ratio at fixed streptavidin concentrations of 14.7 and 22.0 nM. Data were fitted using the Hill−Waud model. (b) Green fluorescence decays of the donor as a result of energy transfer.

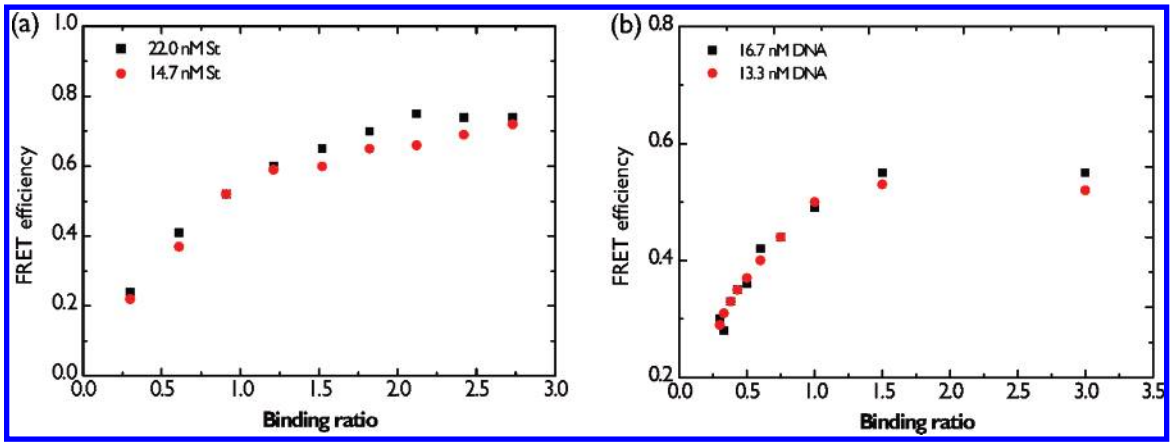

Figure 7. Variation of FRET efficiency as a function of binding ratio for fixed streptavidin concentrations at 14.7 and 22.0 nM (a) and for fixed DNA concentrations of 13.3 and 16.7 nM (b).

To determine binding parameters, the resulting binding curves were fitted to a Hill−Waud model:[23]

$$F = V_{\max}\frac{x^n}{K_H^n + x^n} \tag{2}$$

Here F is the fluorescence intensity, x is the binding ratio, $V_{\max}$ is the maximum binding rate, K_H is the half-dissociation constant, and n is the Hill coefficient of cooperativity. This analysis yielded excellent fits for both curves. The Hill−Waud model fit parameters ($V_{\max}$, K_H, n) were found to be 984, 0.43, and 2.13 for 14.7 nM streptavidin and 1358, 0.43, and 2.13 for 22.0 nM streptavidin, respectively.

To supplement studies at fixed streptavidin concentration, fixed DNA concentrations were also investigated. A flow rate of 100 nM DNA was kept constant, whereas the flow rate of 100 nM streptavidin was varied to generate binding curves. Fixed DNA concentrations were changed from 13.3 to 16.7 nM by varying volumetric flow rates between 0.20 and 0.25 μL min^{-1}. For each fixed DNA concentration, the same set of binding ratios (0.30−3.00) was used. Figure 6b shows a plot of binding ratio versus green fluorescence burst height from the donor detector at 13.3 and 16.7 nM DNA concentrations. As a result of energy transfer, fluorescence bursts of the donor exponentially decay when binding ratios are increased. In addition, the higher the DNA concentration, the higher the donor fluorescence intensity since the streptavidin concentration must be increased when increasing DNA concentration to maintain the binding ratio.

To physically quantify the degree of binding, the burst height intensities, as shown in Figure 7, must be converted to FRET efficiencies. Theoretically, the FRET efficiency (E_{theory}) can be evaluated from the following equation:

$$E_{\text{theory}} = \frac{1}{1 + \left(\frac{R_{DA}}{R_0}\right)^6} \tag{3}$$

Using R_0 = 39.0 Å and R_{DA} = 41.6 Å, the theoretical FRET efficiency was estimated to be 0.4. However, the FRET efficiency can be also experimentally calculated using

$$E_{\text{exp}} = \frac{I'_A}{I'_A + I_D} \tag{4}$$

(23) Moran-Mirabal, J. M.; Edel, J. B.; Meyer, G. D.; Throckmorton, D.; Singh, A. K.; Craighead, H. G. *Biophys. J.* **2005**, *89*, 296−305.

where I_D is the fluorescence intensity of the donor and I'_A is the corrected fluorescence intensities of the acceptor from eq 1. Figure 7 depicts FRET efficiencies obtained from the current experiments. The FRET efficiencies are higher than anticipated from theory due to the fact that the number of donor fluorophores conjugated with streptavidin approximate to 5. When the streptavidin concentration is fixed (Figure 7a), the FRET efficiencies directly depend on the binding ratio. Using a higher streptavidin concentration, but the same binding ratio, results in a shift toward higher FRET efficiencies due to the increased number of both donors and acceptors. FRET efficiency plots obtained at fixed DNA concentrations are shown in Figure 7b. The highest FRET efficiency was obtained at a high binding ratio corresponding to low streptavidin concentrations. The efficiency gradually increases with decreasing streptavidin concentration due to a concomitant increase in the binding ratio. The efficiency was found to be constant when the binding ratio corresponds to ~2.0 for fixed DNA concentrations at 13.3 and 23.3 nM. This is a direct consequence of the limited number of acceptors (or DNA targets).

CONCLUSIONS

We have demonstrated a novel, high-throughput, droplet-based microfluidic assay. The approach allows for online characterization and detection of droplets (defining individual reaction vessels) at rates in excess of 1 kHz. Individual microdroplets (with typical volumes of 300 pl) can be generated in a rapid and reproducible manner and can be monitored and characterized (in terms of their chemical composition) in real time. Application of this system for studying FRET-based DNA assays was successfully achieved using a biotin−streptavidin protocol. We expect that this general approach for high-throughput droplet analysis will be readily extended to the study of other biological assays or molecular interactions such as protein−DNA binding and protein−ligand interactions. Due to the ability to form reproducible small-volume droplets in a rapid fashion, combined with the ability to generate individual droplets of varying reagent composition, studies of biological interactions within droplets at the single-molecule level are an appealing possibility and pave the way for a new generation of droplet-based microfluidic systems. Indeed, we are currently extending our approach to include spatially resolved fluorescence lifetime imaging of droplets. Such developments will facilitate high-throughput, protein-folding studies with sub-microsecond timing resolution. These studies will form the basis of a future publication.

ACKNOWLEDGMENT

This work was supported by the EPSRC and the RCUK Basic Technology Programme. M.S.-A. acknowledges the Royal Thai Government for provision of a research scholarship.

SUPPORTING INFORMATION AVAILABLE

Additional information as noted in text. This material is available free of charge via the Internet at http://pubs.acs.org.

Received for review May 15, 2007. Accepted June 28, 2007.

AC070987O